APPENDIX B

A PLASMA INSTABILITY IN THE SOLAR WIND

06500-6001-R000

3 August 1966

A PLASMA INSTABILITY IN THE SOLAR WIND

by

F. L. Scarf

Space Sciences Laboratory
TRW Systems
Redondo Beach, California

and

J. H. Wolfe and R. W. Silva

Space Sciences Division
Ames Research Center
Moffett Field, California

Prepared for Presentation

at the

Inter-Union Symposium on Solar Terrestrial Physics
Belgrade, Yugoslavia

Space Sciences Laboratory
Systems Laboratories

TRW SYSTEMS
One Space Park
Redondo Beach, California

A PLASMA INSTABILITY IN THE SOLAR WIND*

by

F. L. Scarf

Space Sciences Laboratory
TRW Systems
Redondo Beach, California

and

J. H. Wolfe and R. W. Silva

Space Sciences Division
Ames Research Center
Moffett Field, California

ABSTRACT

Recent solar wind measurements on the Pioneer 6 spacecraft reveal that, in general, the proton velocity distribution is highly anisotropic with $T_{\parallel} > T_{\perp}$, where the subscripts refer to direction with respect to the interplanetary magnetic field. A mechanism which can produce such an anisotropy is considered, and the consequences of this particle distribution with respect to stability of the plasma are analyzed. It is shown that a generalized form of the firehose instability must occur, with growth of magnetosonic (whistler mode) waves near the ion cyclotron frequency. Growth rates are computed for a range of wave frequencies and distances from the sun, and these predictions are compared with available interplanetary power spectra.

*To be presented at the Inter-Union Symposium on Solar Terrestrial Physics, Belgrade.

I. Introduction

In his original paper on the theory of the solar wind, Parker (1958a) predicted that plasma instabilities would develop as the mean free paths became large, and he speculated that wave-particle interactions associated with these instabilities would control the particle distributions in the collisionless region far from the sun. In particular, the possible occurrence of field-aligned thermal anisotropies was considered, and it was argued that extreme values of the anisotropy should not arise because long wavelength magnetohydrodynamic oscillations, triggered by instabilities associated with the velocity space anisotropy (Parker, 1957; 1958b), would randomize the distributions by wave-particle scattering.

Until very recently no detailed measurements of the actual interplanetary particle distributions were available and little effort was devoted to study of microscopic plasma processes in the solar wind. Instead, the collisionless interplanetary plasma was treated as a single magneto-fluid, and various hydrodynamic concepts were widely discussed. However, vector measurements of the positive-ion distributions in the solar wind are now provided by the Ames Research Center plasma probe on Pioneer 6, and they yield fairly complete information about the degree of thermal anisotropy, (Wolfe, et al., 1966). In this note we examine the consequences of the observed velocity space anisotropy with respect to the microscopic stability of the solar wind plasma.

In Section 2 the unique features of the ARC Pioneer 6 plasma probe are briefly discussed and some representative angular and energy distributions for the positive ions in the solar wind are displayed and analyzed. It is shown that the thermal anisotropy generally has $T_{\parallel} > T_{\perp}$, and the possible origin of this distribution is considered.

This anisotropy can place the plasma in the unstable region with respect to Parker's long wavelength (mhd) stability criteria, and the next section contains a detailed analysis of the interplanetary plasma instability. It is shown that the mhd treatment does not suffice, and the Boltzmann equation is used to demonstrate that the fastest growing waves are magnetosonic (whistler mode) oscillations with frequencies near the proton gyrofrequency. Growth rates are computed for a range of values of frequency, distance from the sun, and density at fixed distance. The predictions are compared with available interplanetary power spectra for magnetic oscillations.

It is found that in the quiescent wind the initial growth rates can be small enough so that the wave-particle scattering does not destroy the large anisotropy by the time the wind reaches 1 A.U., but it is argued that disturbances in the wind should trigger very rapid wave growth. Some of the implications of these results are summarized in the concluding section.

2. Positive Ion Distributions in the Solar Wind

The Pioneer 6 spacecraft has several characteristics which make it well suited as a platform for a high resolution plasma probe. The spacecraft was designed to be spin stabilized with the spin axis oriented normal

to the ecliptic plane so that angular scans in ecliptic longitude could be obtained by the natural rotation of the vehicle. Furthermore, the spacecraft was designed to transmit at a relatively high bit rate for an extended period of time (the maximum rate of 512 bits/sec was actually maintained for the first seventy-five days in interplanetary space) and this allowed the ARC plasma probe to be constructed to measure both the incident energy and the polar direction of arrival in a suitably short scan sequence.

The physical characteristics of the ARC Pioneer 6 detector are shown in Fig. 1. The quadrispherical electrostatic analyzer plates guide charged particles within a given energy/unit charge range to a set of eight collectors. Study of the relative currents in these collectors provides the angular distribution of the incident flux in ecliptic latitude (i.e., in polar angle θ). As the spacecraft rotates, these measurements are repeated in fifteen unequal azimuthal sectors (eight fine, seven coarse divisions) and this yields the angular distribution in ecliptic longitude (i.e., angle ϕ, measured with respect to the sun-probe line). Finally, the complete angular scan is repeated in each of sixteen different energy/unit charge windows, $\Delta(E/Q)$. In each positive ion sequence the ARC plasma probe reports the current in 1920 combinations of $\Delta\phi$, $\Delta\theta$, and Δ (E/Q), and thus yields fairly complete information on the vector distribution function.

The high angular resolution available with the 120 combinations of $\Delta\phi$, $\Delta\theta$ on Pioneer 6 evidently represents a considerable improvement

with respect to many previous experiments. For instance, plasma probes mounted on attitude controlled spacecraft were designed to measure plasma from a stabilized sun-oriented platform. The probes were mounted to look at the sun with an angular window in one direction, and they respond to the total integrated current in that direction. For this kind of stabilized system little or no directional information is obtained, and the peak flux is not even measured when the velocity vector associated with this peak deviates significantly from the normal or radial direction.

The previous ARC quadrispherical plasma probes on spin-stabilized spacecraft had some capability for measuring the azimuth angle (in spacecraft coordinates) but because of telemetry restrictions, the sectors were rather coarse. Furthermore, the spin axes were not aligned with respect to the anticipated solar wind direction and single collectors had to be used to give the total current integrated over the spacecraft polar angle. Thus, on the IMP series the azimuth range of 2π was divided into only three large sectors, and peak reading detectors gave the actual peak fluxes within these sectors without indicating the local direction of arrival (Wolfe, Silva, and Myers, 1966). On Explorer 14 similar instrumentation was used with much finer sector widths ($\Delta\phi \sim 13°$) but very limited observations of the solar wind were possible only during a single somewhat disturbed period, and, as on the IMP's, no information about the polar direction of arrival was available (Wolfe and Silva, 1965).

The preliminary report on the ARC Pioneer 6 plasma observations (Wolfe et al., 1966) contains a discussion of several new findings which

could have been obtained only with a high resolution instrument capable of measuring the vector particle distribution. The most significant of these new results are the following:

a) The flow direction of the solar plasma has significant deviations from the expected direction (i.e., nearly radial flow in the ecliptic plane), and fluctuations as high as $\pm$ 5° are observed.

b) The positive ion thermal distribution is not isotropic. In general, the temperature parallel to a vector presumed to be the local magnetic field direction is considerably higher than the perpendicular temperature.

c) Analysis of angular and energy distributions indicates the presence in the solar wind of a third ionic species with charge to mass ratio of four.

These results were illustrated in the preliminary report by the complete display of an extremely complex and relatively unusual distribution taken on December 26, 1965 at a time near 2235 UT (Fig. 3, Wolfe et al., 1966). An easier to interpret representation of a portion of the same data is shown in Fig. 2. Here the energy distribution and the distribution in solar oriented ecliptic longitude are displayed simultaneously for a single collector (number five) which views the ecliptic latitude band from approximately zero to +15°, so that ions incident from just above the ecliptic are detected. In this form, it is clear that there are three separate groups of positive ions with similar angular distributions and different density ratios and values of E/Q. The energy distributions

suggest that these positive ion subgroups have a single bulk velocity vector, with charge to mass ratios of one, two, and four, respectively; they are tentatively identified as H^+, He^{++}, and He^+ ions streaming in the same direction with a common speed, u.

Figure 2 also reveals that the ion groups have a common anisotropic distribution about the bulk velocity vector, $\vec{u}$. In order to come to this conclusion, it is necessary to have sufficiently good angular resolution to be able to decompose the flux in energy window 10 (2184 ev) into separate contributions from the high energy tail of the protons (peaked at approximately 20°W longitude) and the low energy tail of the alpha particles (peaked at approximately 2°E longitude). The significance of these results can be ascertained by making a plot of the speeds and directions of arrival for the various energy windows corresponding to a single species. Figure 3b schematically shows such a plot for quiet periods when the interplanetary conditions are not changing rapidly. It is generally found that during these times the vectors centered closely about the bulk velocity terminate on a nearly straight line, so that in the plasma rest frame the distribution is highly elliptical, as indicated by the scatter diagram in Fig. 3a.

This illustration crudely suggests that the solar wind thermal distribution is highly anisotropic with $\kappa T_\perp$, the random energy in the direction perpendicular to the anisotropy vector, being much smaller than $\kappa T_{//}$. A quantitative analysis of this conjecture has been carried out assuming that in the rest frame the distribution function is a bi-Maxwellian of the form

$$F(\vec{V}) = \left(\frac{m}{2\pi}\right)^{3/2} \frac{1}{\kappa T_{\perp}(\kappa T_{\parallel})^{1/2}} \exp\left\{-\frac{mV_{\perp}^2}{2\kappa T_{\perp}} - \frac{mV_{\parallel}^2}{2\kappa T_{\parallel}}\right\} . \quad (1)$$

This analysis involves several steps: a) Eq. (1) is transformed to yield the distribution function in the spacecraft frame of reference. This very complex expression (See Eq. (2), Wolfe, et al., 1966) gives the currents in the windows, sectors, and collectors as functions of the anisotropy direction (Θ, Φ), the solar wind velocity vector (u, θ, ϕ) and the temperatures, $T_{\parallel}$ and $T_{\perp}$. Aberration corrections for spacecraft orbital motion and the instrument response functions must be inserted at this point. b) The bulk speed u is estimated from analysis of the energy distribution constructed by summing the fluxes in each window, regardless of orientation (note that the IMP and Explorer 14 analyzers were peak reading devices and thus very similar total energy distributions were obtained despite the much cruder angular resolution). c) For fixed u, sample plots of the predicted skewed distributions are prepared for a range of values of the other parameters. To a first very crude approximation, these plots depend only on $K = T_{\parallel}/T_{\perp}$ and Ω, the angle between $\vec{u}$ and the anisotropy direction. Once K and Ω are roughly determined by fitting the observed and predicted skewed distributions, the matching is refined and iterated leading to separate identification of $T_{\parallel}$, $T_{\perp}$, ϕ, θ, Φ, Θ, etc. One preliminary step in this procedure was illustrated in Fig. 5 of Wolfe, et al. (1966), where it was indicated that the December 26, 1965 distribution of Fig. (2) does correspond roughly to a bi-Maxwellian with $u \sim 510$ km/sec, $5 < K < 7$, and $\Omega \sim 60°$. A complete evaluation involves detailed curve fitting since when $T_{\perp}$, $T_{\parallel}$ are finite the straight line skewing shown in Fig. 3b is only valid for velocities fairly close to the mean.

The most reasonable interpretation of the thermal anisotropy is that the temperatures parallel and perpendicular to the local interplanetary magnetic field are unequal. Simultaneous measurement of the interplanetary field on Pioneer 6 suggests that this is indeed the case. As a preliminary analysis, the ratio of the peak currents in collectors 4 and 5 was compared with the instantaneous value of the magnetic field θ-angle (Fig. 6 of Ness, Scearce, and Cantarano, 1966) for the very disturbed period from 2200 UT to 2400 UT on December 26. Qualitative agreement between these quantities was found, and this indicates that the variations in the anisotropy direction do follow the variations in the field orientation. [It should be noted that this point must be verified experimentally since the theoretical hose angle can only be used to predict an average field direction, at best. The actual local field can deviate significantly from the predicted value. Furthermore, the predicted hose angle is only valid on the average if $\vec{u}$ and $\vec{B}$ remain in the ecliptic, and if u_θ is zero.]

The complex distributions observed on December 26, with u and B out of the ecliptic in opposite directions, are relatively infrequent. A much more common case is shown in Fig. 4 where the respective current distributions on collectors 4 and 5 are essentially the same to within one or two telemetry digitizations. This spectrum from December 23, 1965 describes a plasma flow with $\vec{u}$ and $\vec{B}$ almost in the ecliptic plane, and the primary effect of the anisotropy is then to introduce a skewing in solar-oriented ecliptic longitude. Once again, examination of an intermediate E/Q window reveals two kinds of positive ions with the direction

of arrival of the high energy tail of the protons displaced significantly from that of the low energy alpha particles. As before, the small current in the highest E/Q window of the spectrum is detected in an angular sector which indicates that a third ionic species is present; however, this current probably represents an admixture of non-thermal high energy ions and He^+ ions, arriving in the same direction as the solar wind. Figure 4 reveals another complication which is fairly common; although the bulk velocity vector is in the ecliptic plane, it is not radial and the angular shift in $\vec{u}$ is several degrees greater than that anticipated on the basis of normal aberration. This fluctuation is quite analagous to the out-of-ecliptic fluctuation discussed previously, and similar time-varying deviations from the normal are seen in all directions with peak angular amplitudes on the order of 5°. Since the aberration angle is determined by the ratio of the spacecraft orbital speed and the radial component of $\vec{u}$ in the ecliptic, it can be seen that the aberration correction can fluctuate significantly if the direction of $\vec{u}$ varies, even if the incident particle energy remains constant.

These Pioneer 6 results indicate that a plasma probe without adequate energy and angular resolution may not be able to separate species unambiguously, and it may yield an erroneous temperature and distribution shape. It appears that high resolution is also needed to be able to predict the average hose angle accurately, and the ability to make precise aberration corrections requires knowledge of fluctuations in the solar wind flow direction. All of these phenomena can be greatly obscured if

angular scans are taken only in spacecraft azimuth angle, and this is especially true if the spin axis makes a large angle with the ecliptic.

The most plausible source of the large thermal anisotropy generally observed in the Pioneer 6 positive ion spectra would appear to be conservation of the magnetic moment,

$$\mu = \frac{mV_\perp^2}{2B} \tag{2}$$

as the collisionless solar wind (Scarf, 1966) flows outward from the sun. Near the solar equator the mean field magnitude declines with

$$B_r(r) \simeq B_r(r_o) \left[\frac{r_o}{r}\right]^2 ,$$

and

$$B_\theta(r) \simeq \frac{\Omega r}{u(r)} B_r(r) \tag{3}$$

(Parker, 1958a) where $\Omega = 2.94 \times 10^{-6}$ rad/sec. If the field is sufficiently steady on a time scale comparable to an ion gyroperiod, then in the rest frame $\langle mV_\perp^2/2 \rangle = \kappa T_\perp$ declines with B. However, this process is conservative, and the total thermal energy per particle W, should be very nearly constant if no cooperative processes (wave-particle interactions) arise to redistribute the energy. In order to analyze the implications of the large anisotropy observed, we therefore assume that

$$W = \int d^3V \frac{mV^2}{2} F(\vec{V}) \tag{4}$$

is constant, and that $F(\vec{V})$ is locally given by Eq. (1) with N, $T_{||}$ and $T_{\perp}$ slowly varying functions of r; this yields

$$W = \kappa T_{\perp} + \kappa T_{||}/2, \tag{5}$$

so that if μ and W are constant, the $\vec{B}$ variation with r given by Eq. (3) can be used to evaluate the variation in $T_{||}$ and $T_{\perp}$. As an example, we display in Table 1 computed values for B_r, B_θ, B, $T_{||}$, $T_{\perp}$, $K = T_{||}/T_{\perp}$ and $B^2/8\pi N\kappa T_{||}$ which lead to B = 5γ at a 45° angle, N = 5 cm^{-3}, $T_{||} = 10^5$°K, and K = 5 at r = 1 AU (assuming conservation of W and μ). It can be seen that this idealized model can easily account for a 1 AU K-value of 5, since if we work backwards toward the sun, this develops naturally from a distribution which is completely isotropic all the way out to 0.6 AU.

Indeed, it is conceivable that much greater anisotropy factors could develop since proton-proton collisions, which tend to maintain the isotropy, became ineffective much closer to the sun. It has been shown (Scarf, 1966) that the proton mean free path becomes comparable to the thermal scale height near 0.3 AU. If we repeat the calculations leading to Table 1, starting with $T_{\perp}(0.3\ AU) = T_{||}(0.3\ AU) \simeq 1.3 \times 10^5$°K, then the predicted distribution near the earth has K > 21. Thus, even if μ and W are not strictly or continuously conserved, the basic mechanism discussed here should be able to account for the highly anisotropic distributions observed on Pioneer 6.

Table 1. Model Solar Wind Parameters Based on Conservation of Magnetic Moment and Thermal Energy

r(AU)	0.3	0.4	0.5	0.6	0.7	0.8	0.9	1.0
$B_\theta(\gamma)$	11.8	8.84	7.07	5.9	5.05	4.42	3.93	3.54
$B_r(\gamma)$	39.3	22.1	14.15	9.84	7.23	5.53	4.37	3.54
$B(\gamma)$	41.0	23.8	15.8	11.45	8.8	7.07	5.88	5.0
$T_\perp$ (°K)	--	--	--	4.58×10^4	3.52×10^4	2.83×10^4	2.35×10^4	2×10^4
$T_\parallel$ (°K)	--	--	--	4.84×10^4	6.96×10^4	8.34×10^4	9.3×10^4	10^5
K	--	--	--	1.05	1.97	2.94	3.96	5
$\frac{B^2}{8\pi N\kappa T_\parallel}$	--	--	--	5.64	3.16	2.22	1.75	1.45

3. Instabilities Associated with Pressure Anisotoropies

A magnetized collisionless plasma with a significant pressure anisotropy is not generally stable, and waves should grow spontaneously so that wave-particle scattering, which tends to make the distribution isotropic, will develop to remove the instability. Since the ARC Pioneer 6 experiment indicates a large degree of anisotropy near one A.U., it is necessary to analyze these plasma instabilities in some detail in order to determine why the wave-particle scattering has not produced more complete randomization. In this section we examine the appropriate instability, identify the fastest growing waves, compute the associated initial growth rates, and discuss some consequences of these non-linear interactions. Most of the discussion involves the "quiescent" distribution with $T_{\parallel} > T_{\perp}$, although $T_{\parallel} < T_{\perp}$ can certainly occur when the solar wind or interplanetary magnetic field conditions are disturbed.

The first treatment of an instability associated with a thermal anisotropy was based on the mhd equations which are valid in the long wavelength limit. Parker (1957, 1958b) considered a generalized pressure tensor with $P_{ij} = N\kappa T\delta_{ij}$ replaced by

$$P_{ij} = N\kappa T_{\parallel} \left(\frac{B_i B_j}{B^2}\right) + N\kappa T_{\perp} \left(\delta_{ij} - \frac{B_i B_j}{B^2}\right) \tag{6}$$

and he showed that small amplitude solutions to the modified mhd equations satisfy

$$Nm \frac{\partial^2 b}{\partial t^2} \simeq \frac{B_o^2}{4\pi} \left[1 - \frac{4\pi N\kappa (T_{\parallel} - T_{\perp})}{B_o^2}\right] \nabla^2 b \tag{7}$$

where $\vec{B}_o$ is the unperturbed field and $\vec{b}$ is the wave field. If

$$\left(N\kappa T_{\parallel} - N\kappa T_{\perp}\right) > \frac{B_o^2}{4\pi} \tag{8}$$

the system is clearly unstable and the field irregularities grow exponentially with time. This "firehose" instability occurs because the centrifugal acceleration around the curving magnetic field perturbation gives rise to a current which enhances the irregularity.

Instability of a different nature occurs when $T_{\perp}$ exceeds $T_{\parallel}$. In the long wavelength limit, the analog of Eq. (8) is

$$N\kappa(T_{\perp}^2/T_{\parallel}) > B_o^2/8\pi. \tag{9}$$

If this condition is satisfied, the "mirror" instability is triggered. Plasma flows into those parts of the system where the field is weak, increasing $P_{\perp}$ and forcing the field lines farther apart, thus further weakening the field.

The long wavelength stability limits are depicted as functions of $N\kappa T_{\parallel}$, $N\kappa T_{\perp}$, and $B_o^2/4\pi$ in Fig. (5). When the model solar wind parameters of Table 1 are compared with these limits, it can be seen that the nominal parameters lead to a <u>stable</u> situation. For instance, at 1 A.U., Table 1 yields $4\pi N\kappa T_{\parallel}/B_o^2 = 0.315$, $4\pi N\kappa T_{\perp}/B_o^2 = 0.063$, so that Eqs. (8), (9) are not satisfied. Of course, in the actual solar wind there are exceptions to this statement because higher temperatures, larger densities, and smaller magnetic fields are frequently encountered as the wind characteristics fluctuate. Moreover, the density evaluation is probably not absolute because necessary secondary emission corrections are not very well defined.

However, in terms of the classical firehose, the nominal or average anisotropic solar wind is actually stable, and thus the long wavelength oscillations do not seem to be the waves which bind the collisionless solar wind into a fluid.

A complete stability analysis requires examination of the damping and growth rates for finite wavelengths and the Vlasov-Maxwell equations must be used to treat the higher frequencies. For simplicity we restrict the discussion to right hand circularly polarized transverse waves propagating along the interplanetary magnetic field. In the notation of Stix (1962), the dispersion relation $n^2 = R$ has the form

$$n^2 = 1 - \pi \sum_{+,-} \frac{(\omega_p^{\pm})^2}{\omega} \int_0^{\infty} V_\perp^2 \, dV_\perp \int_{-\infty}^{\infty} \frac{dV_\parallel}{(\kappa V_\parallel - \omega - \Omega^{\pm})} \cdot$$

$$\left[\frac{\partial F^{\pm}}{\partial V_\perp} - \frac{k}{\omega} \left(V_\parallel \frac{\partial F^{\pm}}{\partial V_\perp} - V_\perp \frac{\partial F^{\pm}}{\partial V_\parallel} \right) \right] . \qquad (10)$$

Here F is an unperturbed distribution function, $(\pm)$ refers to protons or electrons, $\Omega^{\pm} = \pm (eB/m^{\pm} c)$, and $\omega_p^{\pm} = (4\pi N e^2/m^{\pm})^{1/2}$. The wave field varies as exp (ikz - ωt) with the z-axis parallel to the interplanetary field and n^2 equals c^2k^2/ω^2.

For a cold plasma the zero temperature distributions, $F_o^{\pm} = \delta(V_\perp - \varepsilon)\, \delta(V_\parallel)/2\pi V_\perp$, $\varepsilon \to o$, can be inserted into Eq. (10). The dispersion relation becomes

$$n^2 = 1 - \frac{(\omega_p^{+})^2}{\omega(\omega+\Omega^{+})} - \frac{(\omega_p^{-})^2}{\omega(\omega+\Omega^{-})} \qquad (11)$$

and for $\omega >> |\Omega^-|$, the expression further simplifies to

$$n^2 = 1 + \frac{(\omega_p^+)^2}{\Omega^+(\Omega^+ + \omega)} + \left(\frac{m^-}{m^+}\right)^{1/2} \left(\frac{\omega_p^+}{\Omega^+}\right)^2 + \ldots , \tag{12a}$$

$$\simeq \frac{(\omega_p^+)^2}{\Omega^+(\Omega^+ + \omega)} . \tag{12b}$$

However, when the temperature is finite all values of $V_{\parallel}$ are present and the resonance denominators in Eq. (10) $[(kV_{\parallel} - \omega - \Omega^{\pm})^{-1}]$ generally yield complex terms. This requires introduction of a complex frequency, $\omega \to \omega + i\gamma$, to account for the phenomenon of cyclotron damping or cyclotron growth, and for low temperatures a perturbation expansion can be carried out to obtain the initial growth rate, γ. To lowest order in the thermal effects ω is still given by Eq. (11), (12), and the low frequency expression for γ with $n^2 = R$ is (Kennel and Petschek, 1966)

$$\gamma = -\frac{\pi^2}{k} \frac{(\omega+\Omega^+)^3}{(1+\omega/2\Omega^+)} \int_0^\infty V_\perp dV_\perp F^+(V_\perp, V_\parallel = V_R)$$

$$\times [A^+ + \omega/(\Omega^+ + \omega)] \tag{13}$$

where

$$A^+ = \left. \frac{\int_0^\infty V_\perp dV_\perp \left(V_\parallel \frac{\partial F^+}{\partial V_\perp} - V_\perp \frac{\partial F^+}{\partial V_\parallel}\right) \frac{V_\perp}{V_\parallel}}{2 \int_0^\infty V_\perp dV_\perp F^+} \right|_{V_\parallel = V_R} . \tag{14}$$

Here $V_R = (\omega+\Omega^+)/k$ is the resonant proton velocity and a proton traveling along the magnetic field with this speed sees an anomalous Doppler shift so that $\omega' = \Omega^+$, while at the same time the Doppler-shifted (electron) whistler wave appears to have a polarization reversal. The anomalous Doppler shift and the associated interaction between proton beams and whistler mode waves was first discussed in detail by Ginzburg (1960); in the frame of reference of the particle, the wave appears to be coming backwards with a reversed polarization, and protons with $V_{//} \simeq V_R$ can either absorb energy from the whistler mode wave or lose energy to the oscillation. Brice (1964) analyzed the physical mechanisms which produce the energy exchange, Noerdlinger (1964) computed possible growth rates for the instability in the transition region, and Gendrin (1965) recently summarized magnetospheric applications of the interaction.

For a nearly monoenergetic proton beam traveling along the magnetic field, the anomalous Doppler-shift interaction gives rise to growing whistler mode waves with maximum growth rates for frequencies near $2\Omega^+$ (Gendrin, 1965). In a non-streaming warm plasma with $T_{//}^+ > T_{\perp}^+$, similar growth is induced by those protons in the tail of the $T_{//}^+$ distribution which satisfy the resonance condition, but the presence of the remaining particles modifies the growth rates somewhat, and Eq. (10) must be used to evaluate the amplification coefficient. In order to apply this to the solar wind, we insert Eqs. (1), (12b) into Eqs. (13), (14) (electron thermal effects are neglected since $\omega << |\Omega^-|$). The final expression for γ is

$$\frac{\gamma}{\Omega^+} = \pi^{3/2} \left(\frac{B^2}{8\pi N\kappa T_{\parallel}}\right)^{1/2} \frac{(1+X)^{7/2}}{X^2(2+X)} \left(\frac{T_{\parallel}-T_{\perp}}{T_{\parallel}} - \frac{X}{1+X}\right) \exp\left(-\frac{B^2}{8\,N\kappa T_{\parallel}} \frac{(1+X)^3}{X^2}\right) \tag{15}$$

where $X = \omega/\Omega^+$.

For $T_{\parallel} = 5\ T_{\perp}$, all modes with $\omega < 4\Omega^+$ are unstable and typical growth rates for B = 5 gamma, N = 5 cm^{-3} and $T_{\parallel} = 10^5$°K (the r = 1 A.U. parameters of Table I) are shown in Fig. (6). In the rest frame of the solar wind, the fastest growing waves have $\omega \underset{\sim}{\sim} 1.6\ \Omega^+$ or $f \underset{\sim}{\sim} 0.12$ c/s and the initial time constant, $\tau = \gamma^{-1}$, is 5.5×10^3 secs $\underset{\sim}{\sim}$ 1.5 hours at the peak frequency. This nominal time constant at 1 A.U. is extremely long compared to any relevant wave periods, but it is quite short compared to the time which the solar wind has spent in the collisionless regime. For instance, a 300 km/sec wind covers the distance between 0.5 and 1 A.U. in approximately 2.5×10^5 secs. Since this time is a factor of 45 greater than τ ($\omega = 1.6\ \Omega^+$, r = 1 A.U.), one must ask why large wave amplitudes did not develop to scatter the protons and destroy the K = 5 anisotropy.

This apparent problem appears much less serious when the actual variation of N, B, and $K = T_{\parallel}/T_{\perp}$ with distance from the sun is taken into account. Let us consider only wave frequencies with X = 1 and examine τ ($\omega = \Omega^+$, r) using the nominal values given in Table I for $r \underset{\sim}{\sim}$ 0.6 - 1.0 A.U. The results are shown in Table II, and negative values of τ represent (stable) cyclotron damping time constants, rather than growth time constants.

Table II

r (A.U.)	0.6	0.7	0.8	0.9	1.0
f_c^+ (c/s)	0.175	0.134	0.108	0.089	0.076
τ (secs)	(-1.74×10^{18})	(-3.35×10^{11})	$1.52 \times 10^{7})$	1.75×10^{5}	5.55×10^{3}

It can be seen that the model solar wind is actually stable until it flows past the orbit of Venus, and the time constants at 0.8 A.U., 0.9 A.U. are on the order of one year and two days, respectively. For all practical purposes, the hypothetical plasma flow described in Table I is stable until r approaches one A.U. The basic reasons for the extreme variation in τ with r are displayed in Table I and Eq. (15). Since $B_r(r)$ and N(r) both vary as r^{-2}, $B^2/N \approx r^{-2}$ when the B_θ component is small, and furthermore, if the magnetic moment and thermal energy are conserved K rapidly decreases with r, so that the frequency range for wave growth shrinks.

The actual values of γ and τ shown in Fig. (6) and Table II must be regarded as relative or illustrative numbers rather than any absolute numerical predictions, and they may easily be in error by gross factors when the physical solar wind is considered. For instance, if r, ω, Ω_c, $T_{\parallel}$, and $T_{\perp}$ are fixed, Eq. (15) shows that

$$\tau(N) = \tau(N_o)\ (N/N_o)^{1/2} \exp\ [\alpha(N_o)\ N_o/N] \qquad (16)$$

and the magnitude of τ depends critically on the value of the local interplanetary density, N. This is illustrated in Fig. (7) where $\tau(N)$ is displayed as a function of N for $1 \leq N \leq 25$ cm^{-3} with B = 5 gamma, $T_{\parallel} = 10^5\ ^0K = 5\ T_{\perp}$, and X fixed at 1.6. The variation in τ with N covers an enormous range, however if N(1 A.U.) $\lesssim$ 6-7, then the previous comments still apply; that is, the time constants for $r \leq 1$ A.U. are sufficiently small compared to relevant travel times, that only moderate wave growth may be anticipated for the average solar wind in this region.

The actual value of the mean quiet-time density at 1 A.U. appears to satisfy this criterion. Neugebauer and Snyder (1966b) reported a normalized average density of 5.4 cm^{-3} during the flight of Mariner 2, and the Stanford propagation experiment on Pioneer 6 yielded a preliminary integrated average of 8-9 cm^{-3}, but this initial estimate included both quiet and disturbed periods (Eshleman, et al., 1966). Considerably higher densities were commonly detected on Mariner 2 as high velocity streams overtook slower ones (Neugebauer and Snyder, 1966a; see also Wolfe and Silva, 1965) but in many cases the high densities (and perhaps temperature increases) were accompanied by modest rises in $|\vec{B}|$ so that $(B^2/8\pi N\kappa T)$ remained relatively uniform. However these parametric correlations have not been studied in detail to date, and significantly enhanced growth rates may well be associated with solar wind disturbance interfaces such as those which arise when an obstacle (a slow stream, the magnetopause, etc.) appears in the flow. Analysis of this situation will certainly be complicated by the onset of other instabilities arising from changes in the magnetic field direction near the interface. For instance, if $T_\perp$ locally exceeds $T_{||}$, the conventional high frequency electron whistler mode instability is triggered (Noerdlinger, 1964; Kennel and Petschek, 1966), and VLF magnetic oscillations observed in the transition region (Holzer, et al., 1965) may be related to this more rapid wave growth. Electrostatic waves may also be generated near an interface by runaway interplanetary electric fields (Scarf, 1966).

All of this discussion refers to initial growth rates for the anomalous Doppler shift instability but when the system is unstable, it is also necessary to consider non-linear effects, wave-particle scattering, and the approach to marginal stability. For the resonance interactions between electron whistler-mode signals and nonrelativistic protons, Brice (1964) has shown that $\Delta W_\perp$, the change in transverse energy of the proton, and ΔW, the change in total energy of the proton, are related by

$$\frac{\Delta W_\perp}{\Delta W} = -\frac{\Omega^+}{\omega}. \tag{17}$$

Thus, when the protons lose energy to the wave (ΔW negative) there is a small increase in $W_\perp$, so that as the instability develops, $K = (T_\parallel/T_\perp)$ decreases. This non-linear phenomenon must proceed until, ultimately, the growth rate drops to zero, and then any wave with frequency ω will experience cyclotron damping rather than growth. However, Eq. (17) still applies in this damping region, so that as W increases at the expense of the wave energy, $W_\perp$ decreases. Thus, the cyclotron damping process actually feeds energy into $\kappa T_\parallel$ at the expense of both the wave energy and $\kappa T_\perp$, and this tends to restore the anisotropy. These considerations strongly suggest that the state of marginal stability is one with a finite thermal anisotropy. Although the precise conditions for marginal stability have not been evaluated, Eq. (17) can also help to explain the persistence of the large K-values observed on Pioneer 6.

However, it has already been noted that significantly higher K-values are kinematically possible if the magnetic moment and thermal energy are strictly conserved, and the discrepancy may be attributable to the presence of a finite non-thermal level for electron whistler mode waves with $\omega \gtrsim \Omega^+$. The apparent relative uniformity of $(B^2/8\pi N\kappa T)$ (Neugebauer and Snyder, 1966a) also suggests that non-linear wave-particle interactions govern the observed thermal distributions, and one might expect a Doppler-broadened version of Fig. (6) to provide crude relative wave amplitudes in interplanetary space. The wave data presently available are quite incomplete, but the measurements which have been made do indeed suggest that interplanetary electromagnetic noise signals have a spectral intensity with a broadened but pronounced peak near Ω^+.

This is shown in Fig. (8) where the composite interplanetary power spectral densities of (dB_θ/dt) and $dB/dt)$, based on Mariner 2 fluxgate measurements (Coleman, 1966) and OGO-1 search coil data (Holzer et al., 1965) are plotted together. It should be noted that Mariner 2 measured the power spectrum of B directly and this has been multiplied by ω^2 to convert it to an equivalent search coil power spectrum. This explains why the Mariner 2 threshold level (dashed line), associated with quantization of the magnetometer output voltages, rises with frequency. In terms of the power spectrum of B itself, the corresponding threshold power density is a constant 9.1 gamma^2 sec. Any power spectral density obtained by formal means which falls below this Mariner 2 noise level is not significant.

The Mariner 2 sampling rate allowed computation of power spectra for $f \leq 1160$ cycles per day, and in this range the results are quite significant: a) the power spectral density of (dB_θ/dt) is well above the threshold level; b) the power spectral density of (dB_θ/dt) is more than an order of magnitude higher than that of (dB/dt). As noted by Coleman, "These results suggest that the variations in the interplanetary field are predominantly changes in field orientation rather than in magnitude of the field. Thus, the variations in the different vector components were evidently at least partially coherent." This suggests that the oscillations are indeed transverse circularly or elliptically polarized waves.

The OGO-1 interplanetary results appear to be consistent with the conjecture that the peak wave intensity is near Ω^+, but the relevance of the data is quite uncertain. The OGO-1 and Mariner 2 results were not simultaneous, OGO-1 has a 12-second spin period, and the interplanetary signals are quite weak and fairly near threshold (M. G. McLeod, R. Holzer, private communication). However, additional evidence exists suggesting that large amplitude waves with periodicities on the order of 10 seconds are readily generated when the wind is disturbed. Indeed, the first spacecraft magnetometer to penetrate the transition region aboard Pioneer 1 detected short intense bursts with $f \sim 0.1$ c/s (Sonett, et al., 1959), and recent observations on the third launch VELA spacecraft (Greenstadt, et al., 1966, Scarf, 1966) support these measurements.

IV Conclusions

It has been shown that the anisotropic positive ion distributions observed with the ARC Pioneer 6 plasma probe can be produced by approximate conservation of magnetic moment and thermal energy as the collisionless solar wind flows outward and the imbedded interplanetary field declines in magnitude. The observed distributions are unstable with respect to generation of low frequency whistler mode waves, but the computed growth times are so long that it is anticipated that violation of these conservation laws should not be complete. Nevertheless, the relative uniformity of $(B^2/8\pi NKT)$ and the observations of significant wave energy density at frequencies near f_c^+ indicate that the instability does proceed in interplanetary space. This suggests that the solar wind can serve as a valuable laboratory in which non-linear plasma phenomena can be investigated directly. For instance, the simple linearized theory indicates that the growth rates and wave frequencies should be extremely sensitive functions of B, K, $B^2/8\pi NKT$, etc., and it will therefore be of interest to examine the plasma properties in "null" field regions, at M-region boundaries, near obstacles (e.g., the magnetosphere boundary or interface regions where very fast streams overtake slower ones), during solar storms, etc. Study of any variation in $\langle K \rangle$ with r should also prove to be of interest. It is clear that analysis of these phenomena requires measurement of the full vector distribution function, and simultaneous observations of local wave patterns should also be available.

Acknowledgments

One of the authors (F.L.S.) has been supported by the National Aeronautics and Space Administration under NASW-1366. We are grateful to P. Coleman, Jr., M. G. McLeod, and R. E. Holzer for helpful discussions about their measurements.

FIGURE CAPTIONS

Figure 1. Geometry of the ARC plasma probe for Pioneer 6.

Figure 2. Positive ion distribution on a single collector (number 5) observed on December 26, 1965 near 2335 UT. The simultaneous current distributions on collectors 4 and 6 are shown in Fig. 3 of Wolfe, et al. (1966).

Figure 3. Schematic representation of the bi-Maxwellian distribution with $\kappa T_{\parallel} = mA_{\parallel}^2/2 > \kappa T_{\perp}$: a) the distribution in the plasma rest frame; b) the same distribution in a frame for which the plasma appears to have a bulk velocity $\vec{U}$.

Figure 4. Positive ion distribution observed on December 23, 1965. The currents on collectors 4, 5 are the same to within one or two telemetry digitizations indicating that the flow and the anisotropy direction are both nearly in the ecliptic plane. The distribution is again skewed, and three ionic species appear to be present (E/Q window seven has contributions from high energy protons and low energy alpha particles incident from different directions). Here the bulk velocity vector has a deviation from the radial direction several degrees greater than that anticipated on the basis of normal aberration.

Figure 5. Stable and unstable regions for long wavelength (mhd) Alfvén and "fast" waves. The nominal solar wind parameters, taken from Table 1, correspond to mhd stability.

Figure 6. Growth rates at r = 1 AU based on Eq. (15) and the parameters of Table 1. Since these waves have group and phase velocities less than the customary solar wind speed, Doppler broadening must be considered when spacecraft measurements are analyzed.

Figure 7. Variation in growth time constant with local density. Here ω, Ω^+, and K are fixed at the values shown.

Figure 8. Interplanetary power spectra. The Mariner 2 spectra and the associated digitization noise level (Coleman, 1966) have been converted into equivalent search coil results, as discussed in the text.

REFERENCES

1. Brice, N., Fundamentals of very low frequency emission generation mechanisms, J. Geophys. Res., 69, 4515-4522, 1964.

2. Coleman, P., Jr., Variations in the interplanetary magnetic field: Mariner 2, Part 1. Observed properties, Submitted to J. Geophys. Res.

3. Eshleman, V. R., and others, The interplanetary electron number density from preliminary analysis of the Pioneer 6 radio propagation experiment, J. Geophys. Res., 71, 3325-3327, 1966.

4. Gendrin, R., Gyroresonance radiation produced by proton and electron beams in different regions of the magnetosphere, J. Geophys. Res., 70, 5369-5383, 1965.

5. Ginzburg, V. L., Certain theoretical aspects of radiation due to superluminal motion in a medium, Soviet Phys. Usp., English Transl., 2 (g), 874-893, June, 1960.

6. Greenstadt, E. W., G. Inouye, I. Green, and D. Judge, Observations of magnetic pulsation-like phenomena at 19 R_e in the solar wind-geomagnetosphere transition region, Trans. Amer. Geophys. Union, 47, 143, 1966.

7. Holzer, R. E., M. G. McLeod, and E. J. Smith, Preliminary results from the OGO-1 search coil magnetometer: Boundary positions and magnetic noise spectra, J. Geophys. Res., 71, 1481-1486, 1966.

8. Kennel, C. F. and H. E. Petschek, Limit on stably trapped particle fluxes, J. Geophys. Res., 71, 1-28, 1966.

9. Ness, N. F., C. S. Scearce, and S. Cantarano, Preliminary results from the Pioneer 6 magnetic field experiment, J. Geophys. Res., 71, 3305-3313, 1966.

10. Neugebauer, M. and C. W. Snyder, Mariner-2 measurements of the solar wind, pp 3-24, The Solar Wind, Ed. R. J. Mackin, Jr. and M. Neugebauer (Pergamon Press, New York) 1966a.

11. Neugebauer, M. and C. W. Snyder, Mariner-2 observations of the solar wind, Part 1. Average properties, preprint, Jet Propulsion Laboratory, Pasadena, California, April, 1966b.

12. Noerdlinger, P. D., Wave generation near the outer boundary of the magnetosphere, J. Geophys. Res., 69, 369-375, 1964.

13. Parker, E. N., Newtonian development of the dynamical properties of ionized gases of low density, Phys. Rev., 107, 923-933, 1957.

14. Parker, E. N., Dynamics of the interplanetary gas and magnetic fields, Astrophys. J., 128, 664-676, 1958a.

15. Parker, E. N., Dynamical instability in an anisotropic ionized gas of low density, Phys. Rev., 109, 1844-1876, 1958b.

16. Scarf, F. L., Wave-particle interactions in the solar wind, Raumfarhtforschung, August, 1966 (in press).

17. Sonett, C. P., D. Judge, and J. Kelso, Evidence concerning instabilities in the distant geomagnetic field: Pioneer 1, J. Geophys. Res., 69, 941-943, 1963.

18. Stix, T., The Theory of Plasma Waves (McGraw-Hill Book Co., New York), 1962.

19. Wolfe, J. H. and R. W. Silva, Explorer 14 plasma probe observations during the October 7, 1962 geomagnetic disturbance, J. Geophys. Res., 70, 3575-3579, 1965.

20. Wolfe, J. H., R. W. Silva, and M. A. Myers, Observation of the solar wind during the flight of IMP-1, J. Geophys. Res., 71, 1319-1340, 1966.

21. Wolfe, J. H., R. W. Silva, D. D. McKibbin, and R. H. Mason, The compositional, anisotropic and nonradial flow characteristics of the solar wind, J. Geophys. Res., 71, 3329-3335, 1966.

PIONEER 6
AMES PLASMA PROBE CONFIGURATION

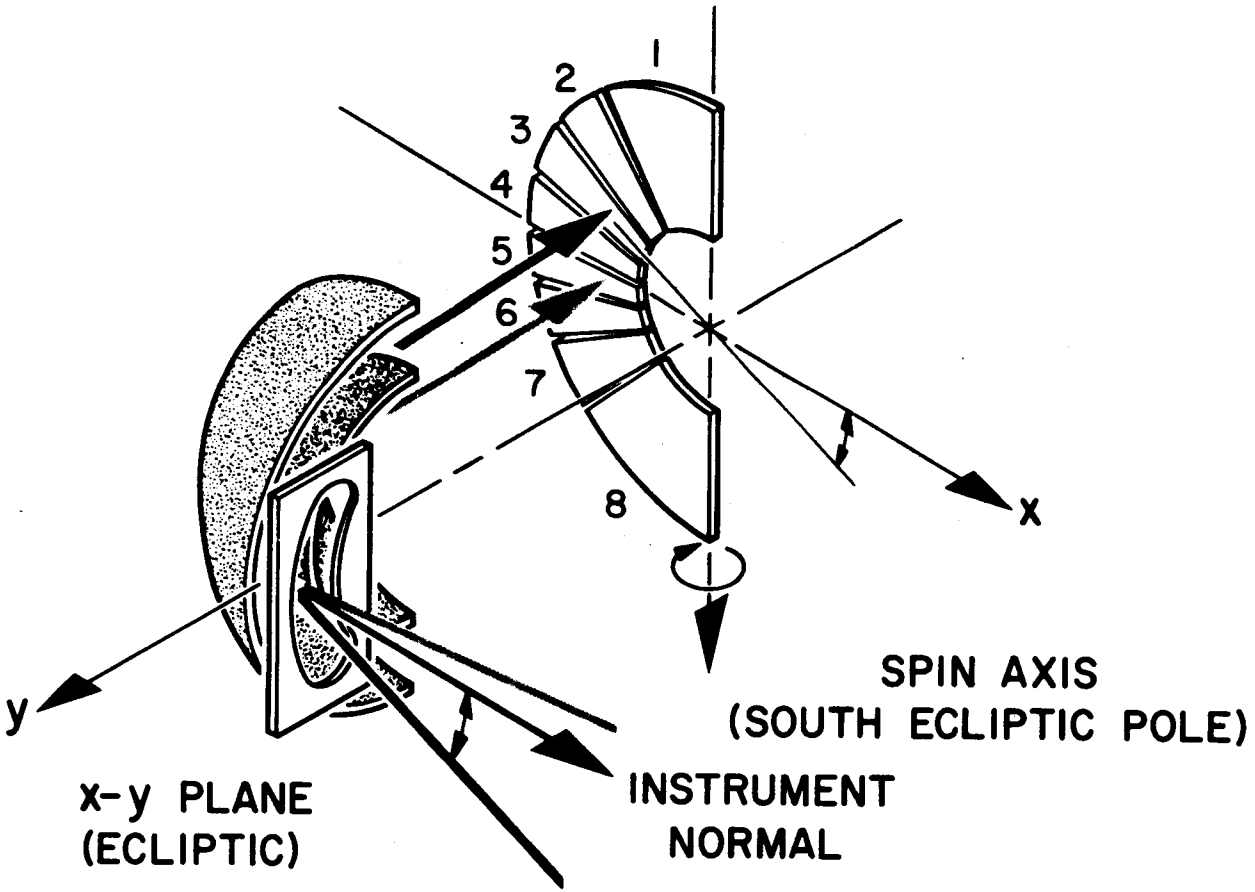

Figure 1

NATIONAL AERONAUTICS AND SPACE ADMINISTRATION
AMES RESEARCH CENTER, MOFFETT FIELD, CALIFORNIA

LONGITUDINAL DISTRIBUTION vs E/Q

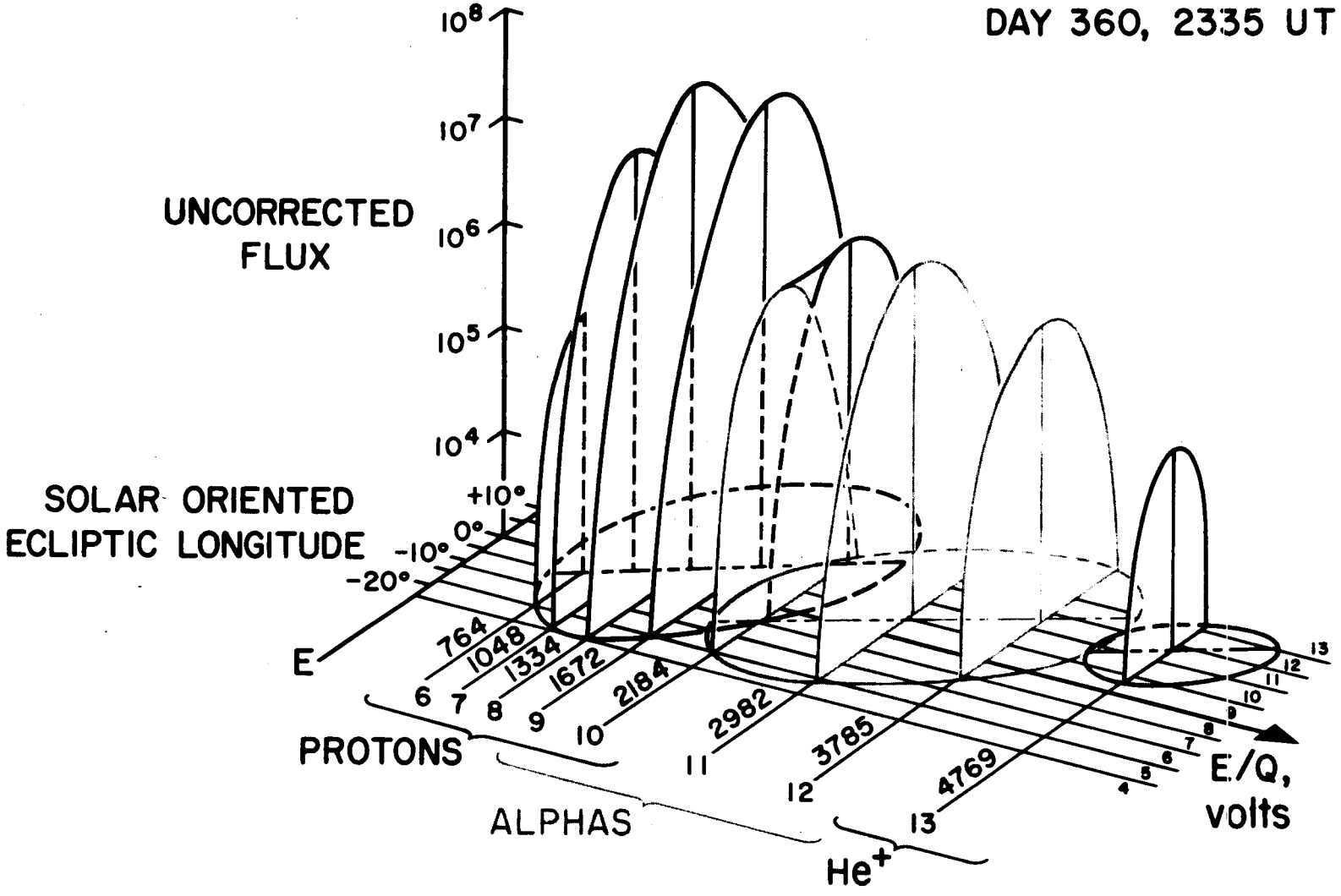

Figure 2

NATIONAL AERONAUTICS AND SPACE ADMINISTRATION
AMES RESEARCH CENTER, MOFFETT FIELD, CALIFORNIA

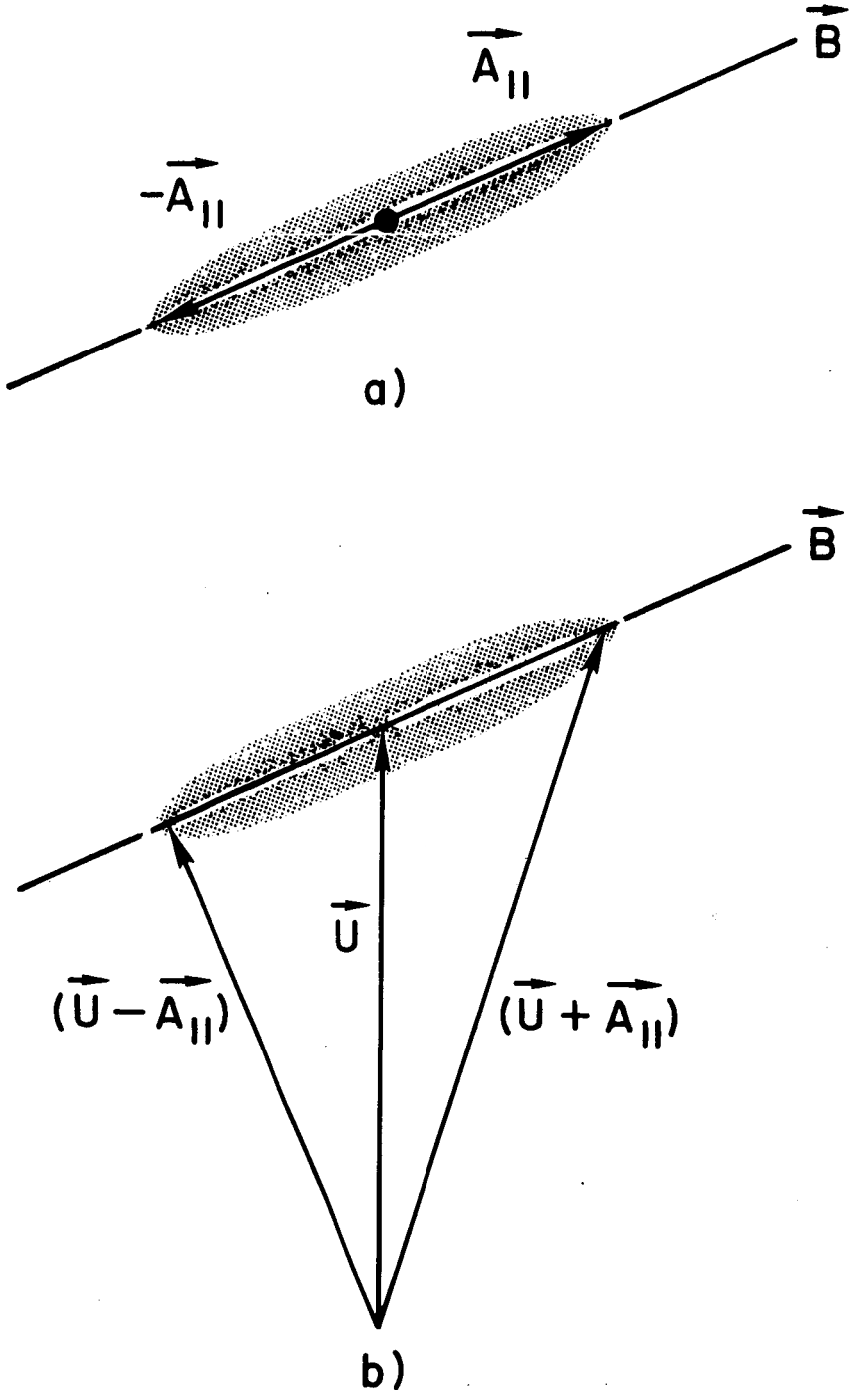

Figure 3

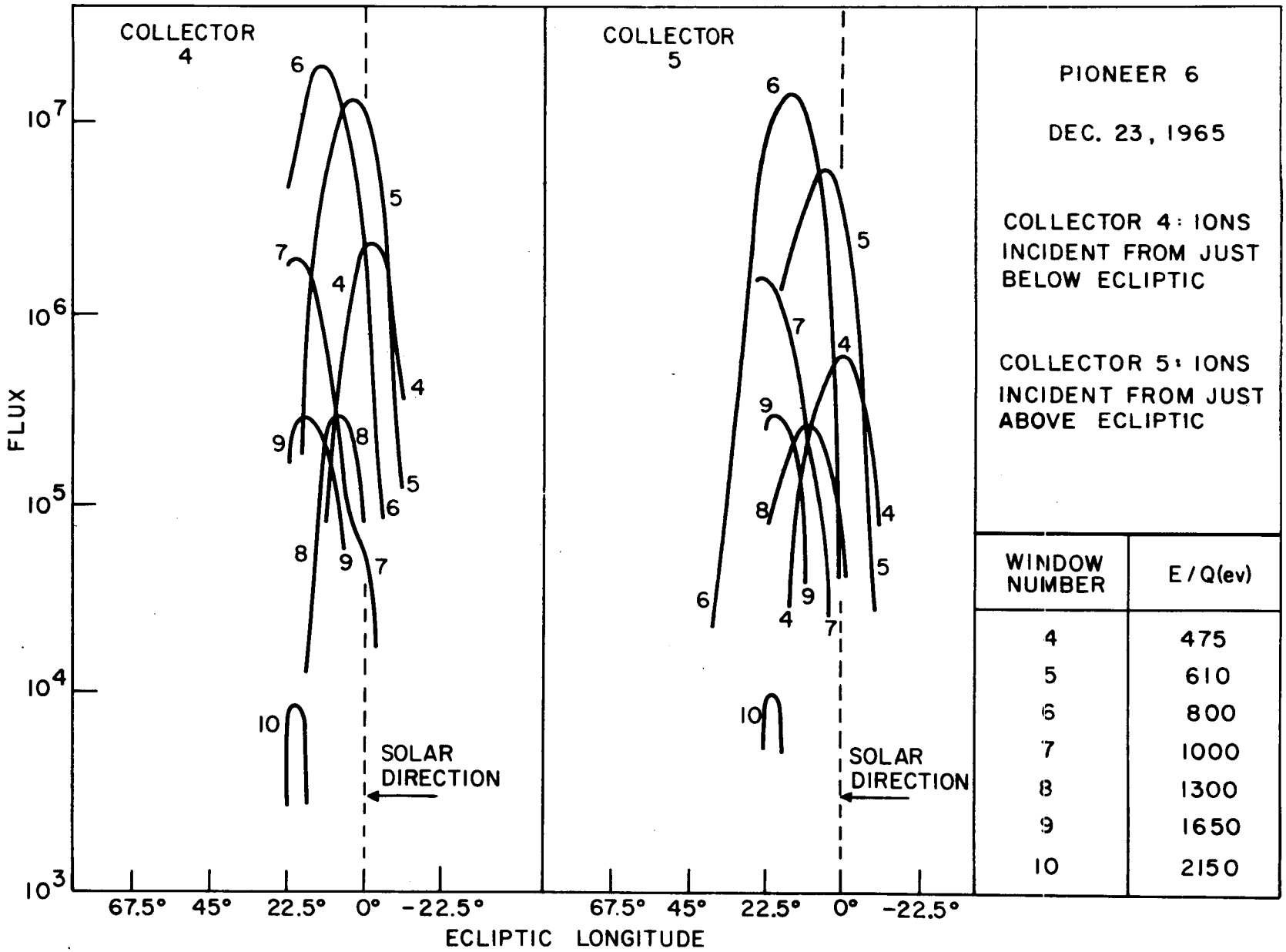
COLLECTOR 4
COLLECTOR 5
PIONEER 6
DEC. 23, 1965
COLLECTOR 4: IONS INCIDENT FROM JUST BELOW ECLIPTIC
COLLECTOR 5: IONS INCIDENT FROM JUST ABOVE ECLIPTIC
WINDOW NUMBER
E/Q(ev)
4 475
5 610
6 800
7 1000
8 1300
9 1650
10 2150
FLUX
10^7
10^6
10^5
10^4
10^3
SOLAR DIRECTION
67.5° 45° 22.5° 0° -22.5°
ECLIPTIC LONGITUDE

Figure 4

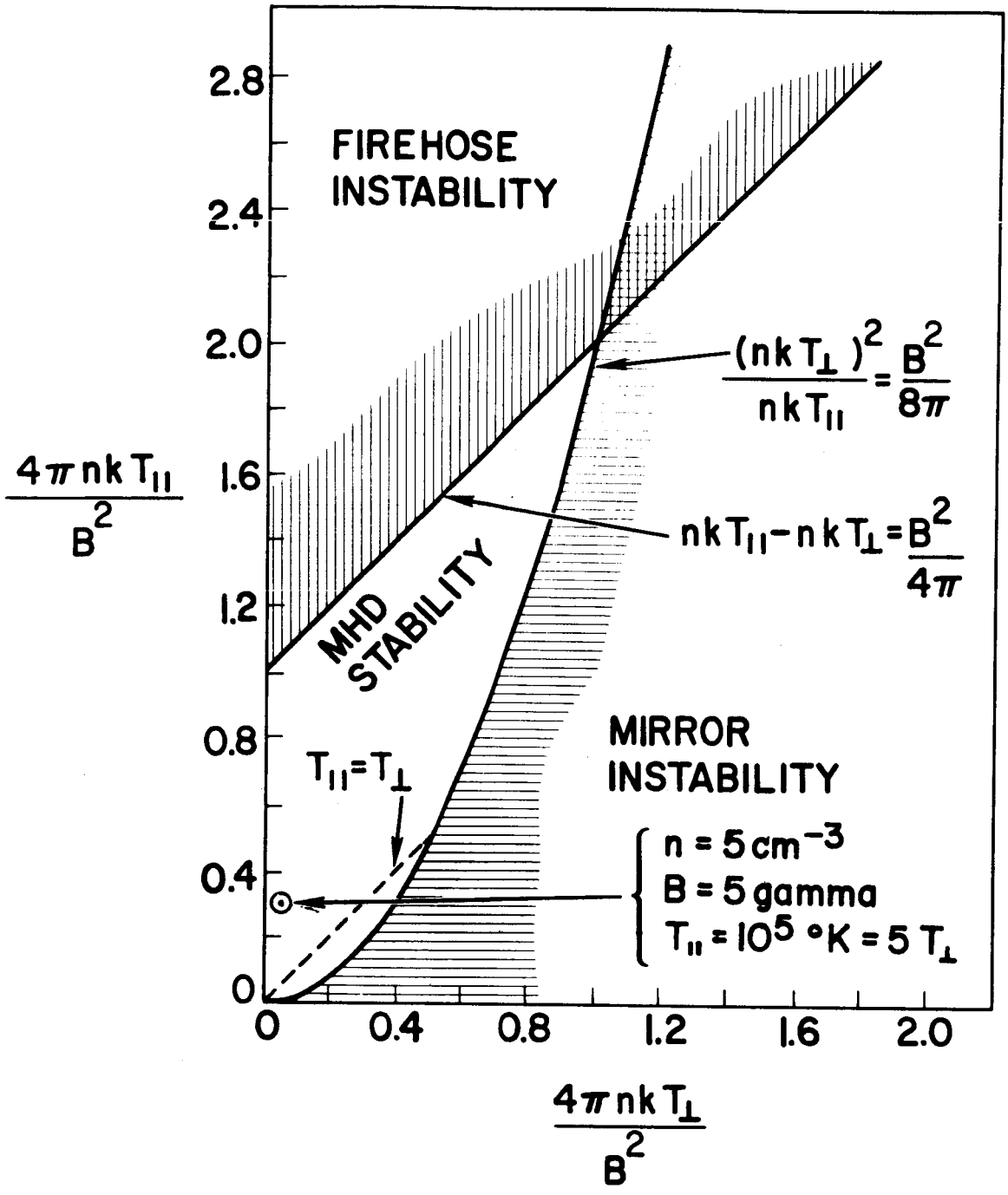
FIREHOSE
INSTABILITY
MHD
STABILITY
MIRROR
INSTABILITY
$\frac{(nkT_\perp)^2}{nkT_{||}} = \frac{B^2}{8\pi}$
$nkT_{||} - nkT_\perp = \frac{B^2}{4\pi}$
$T_{||} = T_\perp$
n = 5 cm^{-3}
B = 5 gamma
$T_{||} = 10^5$ °K = 5 $T_\perp$
$\frac{4\pi nkT_{||}}{B^2}$
$\frac{4\pi nkT_\perp}{B^2}$
0
0.4
0.8
1.2
1.6
2.0
2.4
2.8

Figure 5

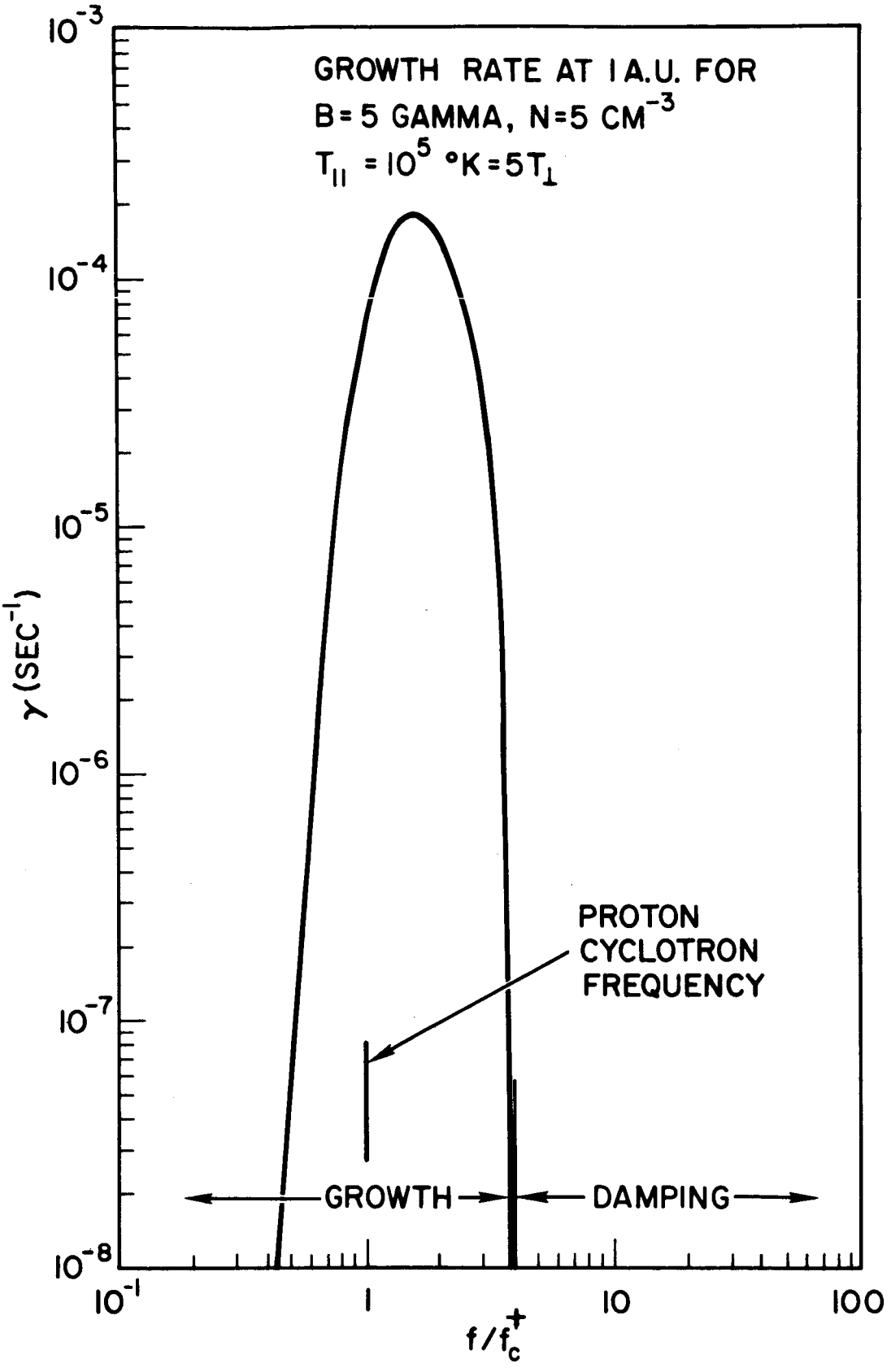
GROWTH RATE AT 1 A.U. FOR
B = 5 GAMMA, N = 5 CM^{-3}
$T_{||} = 10^5$ °K = $5T_{\perp}$
10^{-3}
10^{-4}
10^{-5}
10^{-6}
10^{-7}
10^{-8}
γ (SEC^{-1})
PROTON
CYCLOTRON
FREQUENCY
GROWTH
DAMPING
10^{-1}
1
10
100
f/f_c^+

Figure 6

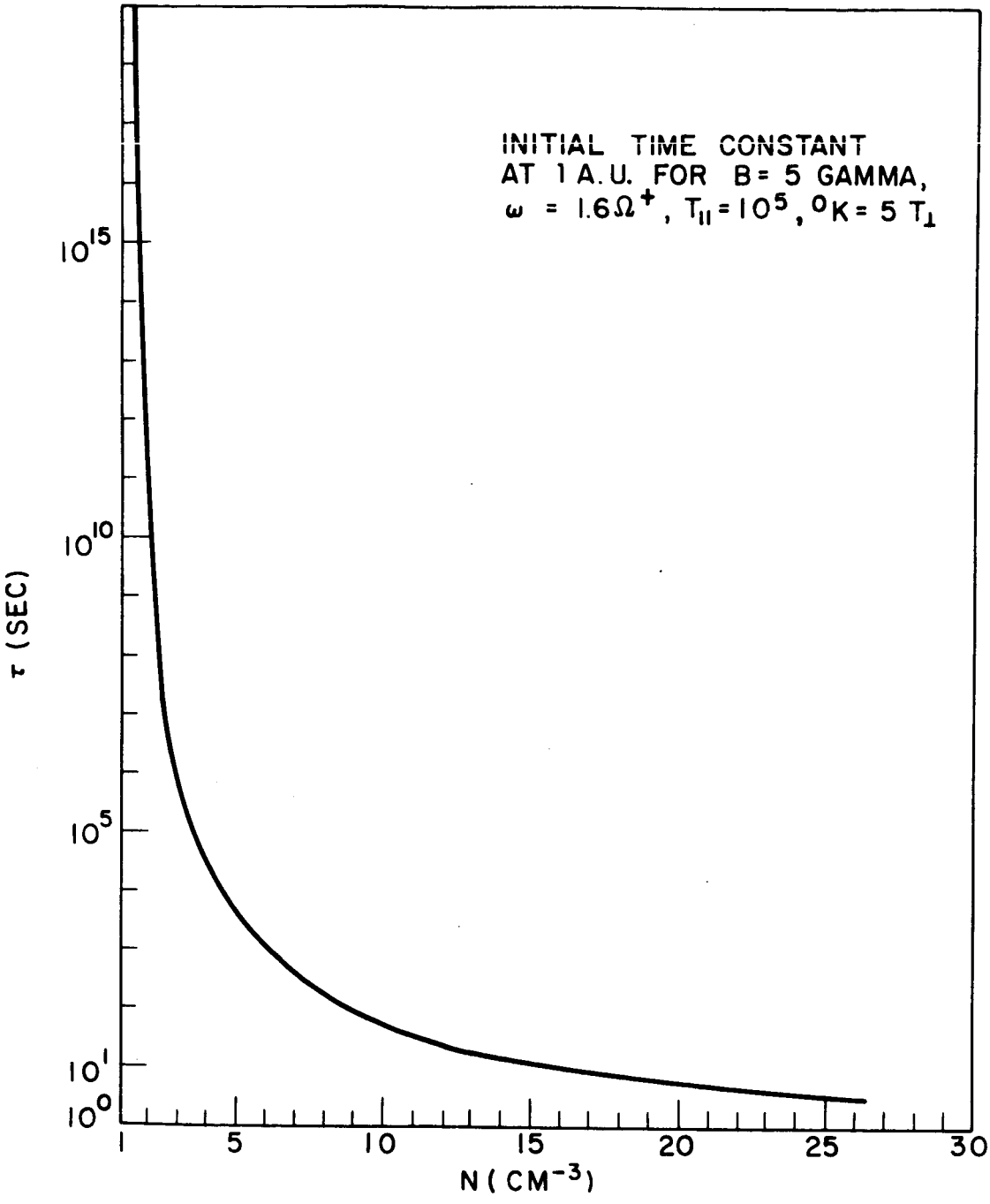
INITIAL TIME CONSTANT
AT 1 A.U. FOR B = 5 GAMMA,
ω = 1.6Ω+, T∥ = 10^5, °K = 5 T⊥
τ (SEC)
10^15
10^10
10^5
10^1
10^0
1
5
10
15
20
25
30
N (CM^-3)

Figure 7

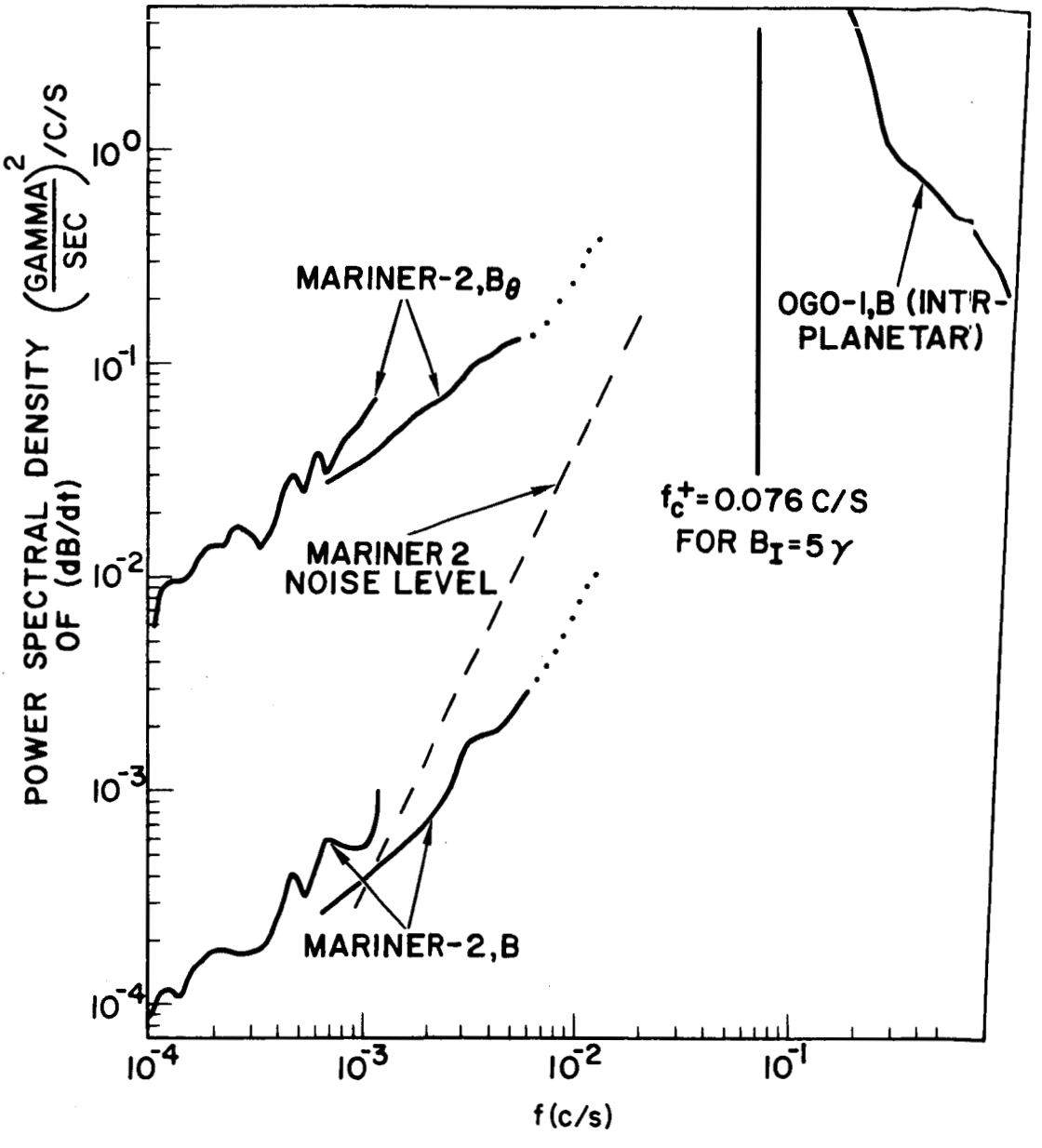
POWER SPECTRAL DENSITY OF $\left(\frac{\text{GAMMA}}{\text{SEC}}\right)^2$/C/S
10^0
10^{-1}
10^{-2}
10^{-3}
10^{-4}
MARINER-2,B_θ
MARINER 2 NOISE LEVEL
MARINER-2,B
OGO-I,B (INTER-PLANETAR)
f_c^+= 0.076 C/S FOR B_I=5 γ
10^{-4}
10^{-3}
10^{-2}
10^{-1}
f(c/s)

Figure 8